A NOVEL ELASTOMERIC BASE ISOLATION SYSTEM FOR SEISMIC MITIGATION OF LOW-RISE BUILDINGS

H. Toopchi-Nezhad [1], M. J. Tait [2], and R. G. Drysdale [3]

[1] *Ph.D. Candidate, Dept. of Civil Engineering , McMaster University, Hamilton, Canada*
[2] *Assistant Professor, Dept. of Civil Engineering , McMaster University, Hamilton, Canada*
[3] *Professor Emeritus, Dept. of Civil Engineering , McMaster University, Hamilton, Canada*
Email: toopchh@mcmaster.ca , taitm@mcmaster.ca, drysdale@mcmaster.ca

ABSTRACT :

An innovative base isolation system for seismic mitigation of ordinary low-rise buildings is introduced in this paper. The proposed base isolation system utilizes "Stable Unbonded Fiber Reinforced Elastomeric Isolator" (SU-FREI) bearings. The steel plates used in conventional laminated rubber bearings are replaced with fiber fabric in FREI bearings. The fiber fabric is extensible in tension and has no flexural rigidity. In an unbonded application, the FREI bearings are simply placed between the superstructure and substructure with no bonding between the contact surfaces. Results from an experimental study conducted on model scale prototype SU-FREI bearings comprised of unfilled soft Neoprene rubber as the elastomer and bi-directional carbon fiber fabric as the reinforcement show that these bearings exhibit Stable Rollover (SR) deformation and perform as an effective seismic isolation device. The experimentally evaluated lateral load-displacement properties of the proposed SU-FREI bearings have been modeled using an iterative analysis with a simplified mathematical model. Results of time history analysis performed on both a 2-storey prototype base-isolated structure and a corresponding fixed-base structure indicate that the proposed base isolation technique can be employed efficiently in hazard mitigation of low-rise buildings located in high seismic regions worldwide.

KEYWORDS: seismic isolation, unbonded application, stable rollover, fiber reinforced elastomeric isolators, low-rise building, masonry structure, laminated rubber bearings

1. INTRODUCTION

Steel Reinforced Elastomeric Isolator (SREI) bearings are currently the most commonly used type of isolator (Naiem and Kelly, 1999). However, their weight and high price has generally limited their application to large and expensive structures. Alternatively, Fiber Reinforced Elastomeric Isolators (FREIs) employ fibers rather than steel plates, as the reinforcement sheet. FREI bearings can provide adequate levels of vertical and lateral stiffnesses as required in a base isolation device. Furthermore, unique aspects such as potentially low manufacturing cost, adequate energy dissipation capability, light-weight, and the possibility of being produced in large rectangular sheets and subsequently cut to the required size, provide promising advantages for this type of bearing. Also, unbonded application of these bearings results in additional advantages through beneficial changes in the bearing's lateral load-displacement characteristics (Toopchi-Nezhad et al. 2007 and 2008).

The base isolation system, introduced in this paper, utilizes square carbon-FREI bearings in an unbonded application. In such an application, FREI bearings, with appropriate aspect ratio, exhibit Stable Rollover (SR) deformation (Toopchi-Nezhad et al. 2007). SR-deformation results in a significant decrease in the lateral stiffness of the bearing and increases its efficiency as a seismic isolator. The unbonded FREI bearings that exhibit SR-deformation are denoted hereafter as stable unbounded (SU) FREI bearings. Results of an experimental study conducted on ¼ scale square SU-FREI bearings, as the prototype base isolators, were used to evaluate the mechanical characteristics of the corresponding full-scale bearings employed in the final design of an isolation system for a prototype low-rise masonry building. An analytical model was developed to simulate the lateral load-displacement hysteresis response of the SU-FREI bearings. The dynamic responses of the Base-Isolated (BI) as well as a corresponding Fixed-Base (FB) prototype building to an input earthquake were studied to verify the seismic mitigation efficiency of the proposed base isolation system.

2. THE PROTOTYPE BASE-ISOLATED BUILDING

A 2-storey masonry building, located in a region with high seismic risk (such as Vancouver, BC, Canada), is considered as a representative prototype superstructure to be seismically isolated. The building is constructed with 20 cm, 15 MPa hollow concrete masonry blocks. To provide a simple and well defined masonry structural system, each shear wall has rectangular cross section with no openings inside and is assumed to be fully grouted. Intentionally, there are no intersections between perpendicular walls. Although a simplified structural system is assumed in this study, its dynamic characteristics are in the same range as real masonry shear wall structures. The base isolation system, which is shown in Fig. 1, consists of 4 square SU-FREI bearings. Compared to conventional SREI bearings, the installation of the SU-FREI bearings is significantly easier as they are simply located between the superstructure and foundation with no bonding at the contact surfaces.

The fundamental natural period of the fixed-base model of the masonry building shown in Fig. 1, along either the x or y directions, was calculated to be 0.17 s. In this analysis, the in-plane lateral stiffness of the masonry shear walls due to bending and shear, was calculated in a model where each wall was considered as a cantilever with both ends fixed against rotation and was subjected to a lateral in-plane load at the top of the storey. To account for cracking in the masonry shear walls, an equivalent thickness was evaluated based on the effective moment of inertia of $I_e = 0.35\ I_g$ as suggested for cracked section properties of beams and walls by the ACI (2002) code. Although the equivalent thickness of the walls (i.e., $t_e = 0.35\ t$) was taken into account for modelling purposes, the weight of the walls was calculated based on their full thickness. The total weight of the building, including the base diaphragm, was found to be around 511 kN. Therefore, each bearing was subjected to approximately 128 kN vertical load.

The ratio of the isolated building period to the fixed-base building period is an indicator of the benefit of a base isolation system in hazard mitigation. In the constant velocity region of the design spectrum, the base shear transmitted to the building decreases as this ratio increases (Naiem and Kelly 1999). Typical earthquake accelerations have dominant periods between 0.1 s and 1.0 s with maximum severity often in the range of 0.2 –

0.6 s. As such, achieving a target isolated building period larger than 1.0 s, being more than 5 times longer than the fixed-base period of the building, is considered suitable.

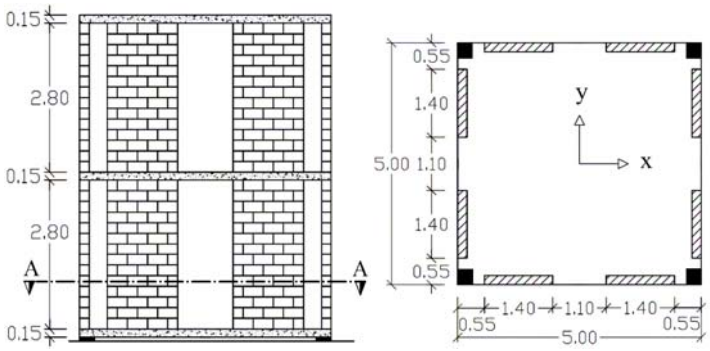

(a) Elevation view (b) Section A-A

Figure 1. The prototype base-isolated masonry building (all dimensions in meter); Solid rectangles in Fig. (a) and solid squares in Fig. (b) represent the SU-FREI bearings

3. GOVERNING EQUATIONS OF MOTIONS

Figure 2 illustrates a simple mass-spring-dashpot idealization used to model the prototype base-isolated building. The base isolation system is modeled using a nonlinear spring k_b, along with an energy dissipation mechanism (damping c_b). Since the superstructure remains nearly rigid when isolated, it can be modeled as a linear elastic system. In order to account for the largest possible response in the superstructure, the linear model considered in this study, conservatively incorporates the cracked section properties for the superstructure. In addition, a 2% equivalent viscous damping ratio for the superstructure is assumed. To study the dynamic response of the corresponding fixed-base building, the same linear stiffness properties of the superstructure in conjunction with a 5% equivalent viscous damping ratio due to larger deformations are assumed in the analysis.

The governing equations for the dynamic system shown in Fig. 2 are as follows (Naiem and Kelly 1999);

$$\boldsymbol{M}^{*}\ddot{\boldsymbol{V}}^{*} + \boldsymbol{C}^{*}\dot{\boldsymbol{V}}^{*} + \boldsymbol{K}^{*}\boldsymbol{V}^{*} = -\boldsymbol{M}^{*}\boldsymbol{r}^{*}\ddot{u}_{g} \tag{3.1}$$

Where,

$$\boldsymbol{M}^{*} = \begin{bmatrix} m + m_b & \boldsymbol{r}^{T}\boldsymbol{M} \\ \boldsymbol{M}\boldsymbol{r} & \boldsymbol{M} \end{bmatrix}, \qquad \boldsymbol{C}^{*} = \begin{bmatrix} c_b & \boldsymbol{0} \\ \boldsymbol{0} & \boldsymbol{C} \end{bmatrix}, \qquad \boldsymbol{K}^{*} = \begin{bmatrix} k_b & \boldsymbol{0} \\ \boldsymbol{0} & \boldsymbol{K} \end{bmatrix}$$

$$\boldsymbol{r} = \begin{Bmatrix} 1 \\ 1 \end{Bmatrix}, \qquad \boldsymbol{r}^{*} = \begin{Bmatrix} 1 \\ \boldsymbol{0} \end{Bmatrix}, \qquad \boldsymbol{V}^{*} = \begin{Bmatrix} v_b \\ \mathbf{v} \end{Bmatrix}, \qquad m = m_1 + m_2$$

where, $\boldsymbol{M}$, $\boldsymbol{C}$ and $\boldsymbol{K}$ are mass, damping, and stiffness matrices of the fixed-base model of the superstructure, respectively. It should be noted that the vertical component of ground motion has been ignored in this analysis. Additionally, the influence of variation in vertical compression on the lateral load-displacement characteristics of the bearings has been neglected. The lateral stiffness of a bearing is generally affected by the value of the vertical compression load. However, experimental results (Toopchi-Nezhad et al., 2007) indicated that when the applied vertical compression load is significantly lower than the buckling load of the bearing, its influence on the lateral stiffness of the bearing can be neglected.

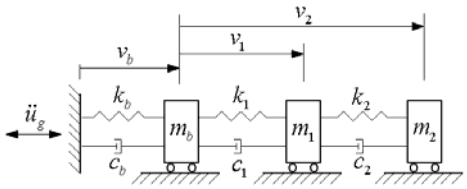

Figure 2. A 3 DOF mass-spring-dashpot idealization of the base-isolated building

4. DESIGN PROPERTIES AND MODELING OF THE SU-FREI BEARINGS

4.1. Outline of an Experimental Study on the ¼ Scale Model of the Bearings

Four ¼ scale square carbon FREI bearings, which had similar plan dimensions of 70 × 70 mm, were designed and constructed. A soft unfilled compound of Neoprene was used as the elastomer material. The total thickness of the model scale bearings was approximately 25 mm of which the total thickness of rubber layers was t_r = 19 mm. The bearings' shape factor (i.e., the ratio of vertically loaded area on one face of the elastomer layer to its perimeter load-free area) was approximately S = 11. The width was 70 mm, and the aspect ratios R (i.e., the ratio of width to the total height of the bearing) was 2.8. Considering the total weight of the base-isolated building (511 kN), each 280 mm × 280 mm full-scale SU-FREI bearing in Fig. 1 would be subjected to a relatively light vertical pressure of 1.6 MPa.

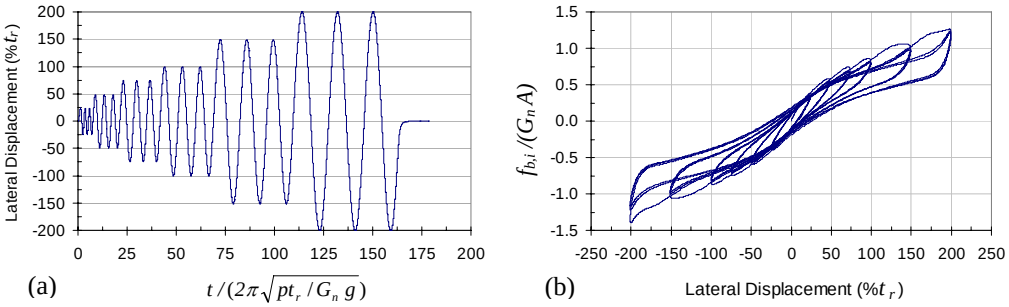

Figure 3. Lateral load-displacement response of ¼ scale bearing, under constant 1.6 MPa vertical pressure; (a) Input signal at 6 different lateral displacement amplitudes ranging from 25 to 200% t_r; (b) Resulting hysteresis loops

An experimental study was conducted on the ¼ scale bearings in order to evaluate their displacement characteristics and damping values as well as to verify their suitability as a seismic isolation device in an unbonded application (Toopchi-Nezhad et al. 2008). To simulate the unbonded boundary conditions of the bearings in the cyclic testing program, the bearings were not attached to the platens of the test machine. Cycling testing was conducted in a displacement control manner. Each bearing was tested under p = 1.6 MPa design constant vertical pressure and was subjected to the lateral displacement time history of Figure 3a. In this figure, time t has been normalized in terms of the nominal base-isolated period of the bearing $T_{b,n} = 2\pi\sqrt{pt_r/G_n g}$. G_n = 0.4 MPa is the nominal shear modulus of the elastomer at 100% strain, and g is the gravity acceleration. Figure 3b shows the hysteresis loops for one of the tested bearings. The bearings lateral load $f_{b,i}$ in Fig. 3b has been normalized by $G_n A$ where, A = 4900 mm^2 is the cross section area of the bearing in the plan view.

As shown in Figure 3b, due to rollover deformation in the bearing, the effective (secant) lateral stiffness decreased significantly with increased amplitude of lateral displacement. However, the observed positive values

of lateral tangent stiffness throughout the hysteresis loops implied that the bearing showed stable rollover (SR) deformation. The SR-deformation in a SU-FREI bearing is achieved as a direct consequence of (i) lack of flexural rigidity in the fiber reinforcement sheets, and (ii) unbonded contact surfaces of the bearings (see Fig. 4). Vertical compression testing revealed that vertical stiffness of the ¼ scale FREI bearings was sufficiently large to eliminate the influence of the rocking vibration modes in the lateral response of the base-isolated building.

(a) 0% t_r (0 mm) (b) 100% t_r (19 mm) (c) 200% t_r (38 mm)

Figure 4. Photographs of one of the model scale SU-FREI bearings taken at different amplitudes of lateral displacement in cyclic testing under constant vertical compression of 1.6 MPa

4.2. Modeling of the full-scale SU-FREI bearings

Lateral load-displacement hysteresis loops of the full-scale bearings can be constructed from Fig. 3b, when the values of t_r = 76 mm, and A = 78400 mm^2 for the full-scale SU-FREI bearings are used. Table 4.1 contains effective lateral stiffness and damping ratios of the bearings at different levels of displacement amplitudes. Although the SU-FREIs were fabricated using a low damped Neoprene with 5% nominal supplier-specified damping, significant damping (8% to 12%) was achieved due to the presence of the fiber reinforcement. Considering the 1.6 MPa design vertical pressure and the values of resulting effective lateral stiffness, the base-isolated period of the bearings, depending to the displacement amplitude, varies between 0.8 to 1.4 s (0.7 to 1.25 Hz). Therefore, the target base-isolated period (1s and longer as stated before in this paper) will be achieved if the full-scale model of the tested bearing are used as the seismic isolators of the given superstructure.

The lateral load $f_{b,i}$ that is experienced by an individual SU-FREI bearing "*i*" in the base isolation system can be attributed to sum of the stiffness and damping forces as follows;

$$f_{b,i}(t) = f_{sb,i}(t) + f_{db,i}(t) \tag{4.1}$$

In a simple approach, the stiffness force $f_{sb,i}(t)$ of each bearing, can be modeled as a polynomial of order 5 given by Eq. 4.2.

$$f_{sb,i}(t) = k_{b,i}(v_b(t))v_b(t) = (b_0 + b_1 v_b(t) + b_2 v_b^2(t) + b_3 v_b^3(t) + b_4 v_b^4(t))v_b(t) \tag{4.2}$$

where, $k_{b,i}(v_b(t))$ is the effective lateral (secant) stiffness of the bearing as a function of lateral displacement $v_b(t)$ at the base isolation system. The 5 parameters b_0 to b_4 are constants to be determined by applying a least squares fit to the experimentally evaluated lateral load-displacement hysteresis loops of the full-scale prototype bearings. In a dynamic analysis, the mathematical hysteresis loops of the bearing can be constructed when an equivalent viscous damping force is added to the stiffness force calculated by Eq. 4.2. A Rayleigh damping idealization that models the energy dissipation of the individual bearings can be expressed as

$$f_{db,i}(t) = c_{b,i}(t)\dot{v}_b(t) \tag{4.3}$$

where, at any instant in time, the bearing's damping coefficient $c_{b,i}(t)$ is calculated based on a constant

equivalent viscous damping ratio of ξ, tributary mass of the structure on each bearing (m_i), and effective lateral stiffness of the bearing, namely $k_{bi}(v_b(t))$ by

$$c_{b,i}(t) = 2\xi\sqrt{k_{b,i}(v_b(t))\,m_i} \tag{4.4}$$

It should be noted that since the base-isolated system is comprised of 4 identical bearings, its lateral stiffness k_b and damping coefficient c_b, to be used in Eq. 4.1, are 4 times larger than $k_{b,i}$ and $c_{b,i}$, respectively.

Table 4.1. Design effective lateral stiffness $k_{b,i}$ (N/mm) and damping ratios ξ (%) of each individual full-scale SU-FREI bearing

Cycle of the test	Lateral displacement amplitude (t_r = 76 mm)											
	25% t_r		50% t_r		75% t_r		100% t_r		150% t_r		200% t_r	
	$k_{b,i}$	ξ	$k_{b,i}$	ξ	$k_{b,i}$	ξ	$k_{b,i}$	ξ	$k_{b,i}$	ξ	$k_{b,i}$	ξ
1st cycle	656	12	493	12	413	10	357	9	292	10	274	9
Last (3rd) cycle	616	12	458	11	381	9	334	9	268	8	246	8

As observed in Fig. 3b, the lateral load-displacement response of the bearings was found to be highly nonlinear. At each level of lateral displacement, the first cycle of the hysteresis loops was attributed to the unscragged response during which the elastomeric bearing exhibited larger lateral load resisting and damping values than in the two following cycles. As a conservative approach, in order to account for the unscragged response properties of the bearings at the peak lateral displacement calculated by the time history analysis, the polynomial of Eq. 4.2 (also called the backbone-curve) was fitted to only the first cycles of the hysteresis loops at each displacement amplitude shown in Fig. 3a. Figure 5a shows the corresponding unscragged (1st cycles) lateral load-displacement hysteresis loops of a full-scale SU-FREI bearing at six different displacement amplitudes ranging from 25% t_r (19 mm) to 200% t_r (152 mm). Also shown in this figure is the backbone-curve fitted to all of the unscragged loops to provide an estimate for $f_{sb,i}$ developed in the bearing (Curve 6). Due to increasing tangent stiffness at 200% t_r, the peak lateral load was accurately predicted by Curve 6 at this extreme lateral displacement amplitude. However, if the peak lateral displacement amplitude of the bearing, calculated by time history analysis, was significantly less than 200% t_r, the maximum lateral load would be underestimated by Curve 6 (see Fig. 5a). Therefore, the model was modified in order to simulate the increased tangent stiffness of the hysteresis loops at peak displacement amplitudes less than 200% t_r (152 mm).

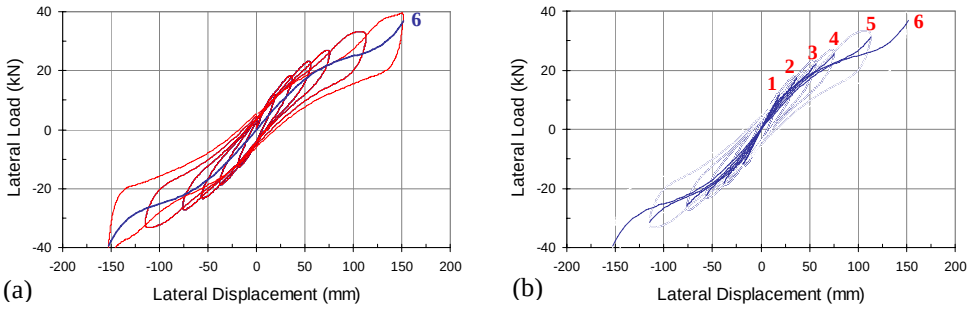

Figure 5. Lateral load-displacement response of the individual full-scale SU-FREI bearings; (a) Unscragged (1st cycle) hysteresis loops (inferred from lateral cyclic testing on the ¼ scale model of the bearings); (b) Backbone-curves resulted from curve fitting (used to model the stiffness force of the SU-FREI bearings)

Figure 5b shows a set of backbone-curves, namely Curves 1 to 6, each fitted to the first cycle hysteresis loops, that are shown in Fig. 5a, up to a specified lateral displacement. For example, Curve 5 has been fitted to all first cycle hysteresis loops from 25% t_r up to 150% t_r (114 mm) lateral displacement. Table 4.2 contains the corresponding b-parameters for Curves 1 to 6. In the time history analysis presented in this paper, the

appropriate values of the b-parameters together with a proper viscous damping ratio are determined through an iterative approach. The following is a description of the iterative approach employed. i) The b-parameters of Curve 6 are initially used to model the bearings' stiffness. Additionaly, a damping ratio of ξ = 8% corresponding to 200% t_r lateral displacement is assumed. ii) Time history analysis of the base-isolated structure is carried out and the peak amplitude of the bearings' lateral displacement ($v_{b,\max}$) is calculated. iii) The new b-parameters and ξ-value are calculated from Table 4.2 through linear interpolation between the values corresponding to the lateral displacement levels that bracket the current $v_{b,\max}$. iv) The value of $v_{b,\max}$ is updated through repeating the time history analysis on the base-isolated structure. v) This iterative process is continued until $v_{b,\max}$ converged to its unique value with sufficient accuracy. Using this technique in the time history analysis described in the next section, the convergence of $v_{b,\max}$ with an accuracy of 1% t_r, was achieved after 3 iterations.

Table 4.2. b-parameters for the backbone-curves shown in Fig. 5b

Curve	$v_{b,max}$	ξ (%)*	b_0	b_1	b_2	b_3	b_4
1	25% t_r (19 mm)	12	$6.63762e^{-01}$	$-3.91637e^{-03}$	$-2.05829e^{-04}$	$9.92181e^{-06}$	$2.85860e^{-07}$
2	50% t_r (38 mm)	11	$6.22710e^{-01}$	$-4.33525e^{-04}$	$-2.94231e^{-04}$	$3.63891e^{-07}$	$1.35992e^{-07}$
3	75% t_r (57 mm)	9	$5.31905e^{-01}$	$-1.80998e^{-04}$	$-1.08943e^{-04}$	$5.54897e^{-08}$	$2.08792e^{-08}$
4	100% t_r (76 mm)	9	$4.73049e^{-01}$	$-1.08228e^{-04}$	$-5.49765e^{-05}$	$1.92699e^{-08}$	$5.53341e^{-09}$
5	150% t_r (114 mm)	8	$4.28254e^{-01}$	$-6.61779e^{-05}$	$-3.07449e^{-05}$	$6.62940e^{-09}$	$1.46255e^{-09}$
6	200% t_r (152 mm)	8	$3.84435e^{-01}$	$1.12916e^{-05}$	$-1.92066e^{-05}$	$-2.02357e^{-09}$	$5.79201e^{-10}$

* Minimum achieved damping ratios at each level of lateral displacement amplitude selected from Table 4.1

5. TIME HISTORY ANALYSIS

A time history analysis is performed to demonstrate the seismic mitigation effectiveness of the proposed base isolation system. The acceleration time history for the NS component of El Centro 1940 earthquake was selected and scaled by a factor of 1.32 to match its Peak Ground Acceleration (PGA) to the maximum expected value (with 2% probability of exceedence in 50 years) for Vancouver, namely 0.46g (NBCC, 2005). Comparison between the 5% damped pseudo acceleration spectrum of this earthquake and the design spectrum for Vancouver (for site class C (very dense soil or soft rock) as defined by NBCC, 2005) showed that for the periods longer than approximately 0.2 s, the input earthquake overestimated the expected level of seismic hazard.

Figure 6a shows the lateral load-displacement hysteresis loops for each of the SU-FREI bearings in the base isolation system, resulting from time history analysis, and Fig. 6b contains the time histories of base shear in the base isolated building and the corresponding fixed base model.

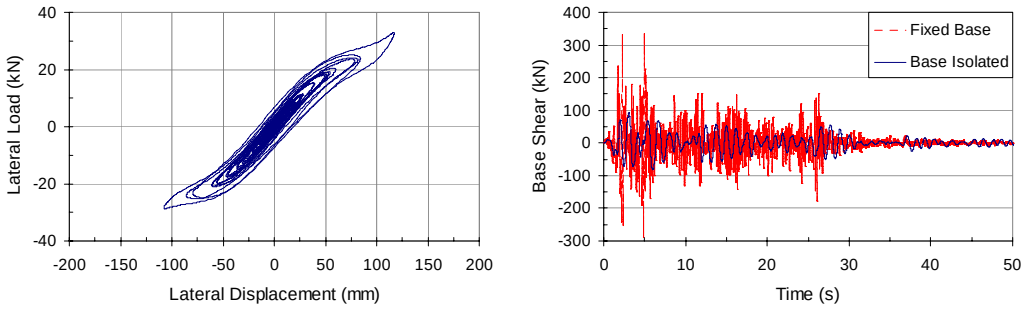

(a) Hysteresis loops in the SU-FREIs (b) FB versus BI buildings

Figure 6. Results of time history analysis

Table 5.1 lists the peak response values for both the fixed-base and base-isolated buildings. Significant decreases

in the peak response values for the base-isolated system with respect to those for the corresponding fixed-base model indicate that the base isolation system proposed in this study performs effectively. A minimum overturning safety factor of 3.2 in the base-isolated building implies that no detachment at the contact surfaces of the bearings has occurred.

Table 5.1. Peak response values of the fixed-base (FB) and the base-isolated (BI) masonry building

	Absolute Accel. (g)		Inter-Storey Drift (mm)		Base Shear (kN)	Overt. Moment (kN.m)
	1st Floor	Roof	1st Storey	2nd Storey		
FB model	0.78	1.16	5.7	3.0	334	1462
BI model	0.26	0.26	1.6	0.7	94	399
Response Reduction	66.7%	77.6%	71.9%	76.7%	71.9%	72.7%

6. CONCLUSIONS

Results of a time history analysis performed on both a fixed-base and a base-isolated model of a prototype masonry shear wall structure, representative of a typical small low-rise building, are presented in this paper. Novel "Stable Unbonded Fiber Reinforced Elastomeric Isolator" (SU-FREI) bearings were utilized in the proposed base isolation system. A model was presented to simulate the experimentally evaluated lateral load-displacement response properties of the bearings. Analytical results indicated that the SU-FREI bearings can effectively decrease the seismic demand on typical low-rise buildings constructed in high seismic risk region such as Vancouver, Canada. SU-FREI bearings have significant potential to be considered as a cost effective base isolation system for many structures including ordinary housing, if they are made through a mass production manufacturing technique and are supplied as a catalogue commodity.

ACKNOWLEDGEMENT

This research was carried out as part of the mandate of the McMaster University Centre for Effective Design of Structures funded through Ontario Research and Development Challenge Fund. The authors also would like to gratefully acknowledge additional funding from the Ministry of Science, Research and Technology (MSRT) of Iran and the Natural Sciences and Engineering Research Council of Canada (NSERC).

REFERENCES

ACI. (2002). Building Code Requirements for Structural Concrete and Commentary, American Concrete Institute, ACI 318-02.

ASCE. (2005). Minimum Design Loads for Buildings and Other Structures, American Society of Civil Engineers, ASCE/SEI 7-05.

Naeim, F., and Kelly, J.M. (1999). Design of Seismic Isolated Structures, John Wiley, New York.

NBCC. (2005). National Building Code of Canada. Institute for Research in Construction, National Research Council of Canada, Ottawa, Ontario.

Toopchi-Nezhad H., Tait M.J., and Drysdale R.G. (2007). Testing and modeling of square carbon fiber reinforced elastomeric seismic isolators. *Journal of Structural Control and Health Monitoring,* DOI: 10.1002/stc.225.

Toopchi-Nezhad H., Tait M.J., and Drysdale R.G. (2008). Lateral Response Evaluation of Fiber Reinforced Neoprene Seismic Isolators Utilized in an Unbonded Application. *Journal of Structural Engineering, ASCE,* 134:10.